

Collisions and inhomogeneous forces between solitons of different dimensionality

Eugenio DelRe

Fondazione Ugo Bordoni, Via B. Castiglione 59, 00142 Rome, Italy, and
Istituto Nazionale Fisica della Materia, Unità di Roma "La Sapienza," Rome, Italy

Stefano Trillo

Department of Engineering, University of Ferrara, Via Saragat 1, 44100 Ferrara, Italy, and
Istituto Nazionale Fisica della Materia, Unità di Roma III, Via della Vasca Navale 84, 00146 Rome, Italy

Aharon J. Agranat

Department of Applied Physics, Hebrew University of Jerusalem, 91904 Jerusalem, Israel

Received November 29, 1999

We exploit nonlinear propagation in photorefractive crystals to observe the phenomenology associated with the collision and interaction of solitons of different transverse dimensions: a self-trapped stripe and a round soliton. Along with evidence of particlelike behavior, our results indicate the emergence of a new phenomenology related to the hybrid-dimensional system. © 2000 Optical Society of America

OCIS codes: 190.5530, 190.5330.

Interactions and forces between solitary waves (see, e.g., Refs. 1–4) are of crucial importance not only with respect to applications but also because the very definition of a soliton is commonly associated with its additional property of exhibiting elastic particlelike collisions. In this Letter we experimentally tackle, for the first time to our knowledge, a fundamental issue that is meaningful for spatial solitons (henceforth used as a synonym for solitary waves): the interaction among solitons of different dimensionalities. To date, spatial soliton scattering has been studied theoretically (see, e.g., Refs. 5 and 6) and experimentally^{2,7–10} only for solitons of the same dimensionality. Here, a one-dimensional (1 + 1D) soliton (slab or stripe soliton) is made to interact with a two-dimensional (2 + 1D) soliton (needle or round soliton). The collision is supported by the photorefractive screening nonlinearity¹¹ that permits simultaneous observation of stripe and needle self-trapping. Results indicate solitonic behavior under the proper conditions. More importantly, we observe a new phenomenology that stems from the inherently inhomogeneous nature of the interaction forces in the transverse plane, which in turn is due to the different symmetries of the interacting particles. Numerical results corroborate our belief that these basic features are ubiquitous, not qualitatively dependent on the particular nonlinearity.

Experiments are performed in which narrow (diffracting under linear conditions) laser beams are launched into a biased photorefractive centrosymmetric crystal. This system exhibits spatial self-trapping of slab beams¹² and needle beams¹³ when the parameters of each single beam obey appropriate conditions for existence^{12,13} that are in close analogy to those of noncentrosymmetric spatial screening solitons.¹¹ The experimental apparatus is shown in Fig. 1. Three separate beams are made to impinge upon a 2.4-mm-long sample of paraelectric potassium lithium tantalate niobate (KLTN; see Refs. 12 and 13 for sample

details) kept at a constant temperature $T = 21^\circ\text{C}$ and subject to an external voltage V , engendering a field along the principal x axis. The beams are combined by two nonpolarizing 50/50 beam splitters. The background beam is a collimated y -polarized beam of approximately 8-mm intensity FWHM obtained from an argon-ion laser operating at $\lambda = 514\text{ nm}$. The beam that forms the slab soliton is obtained from the same laser but is x polarized and focused along x onto the input facet of the sample by means of an $f = 150\text{ mm}$ cylindrical lens. An x -polarized needle beam is obtained either from the same laser for coherent interactions or from a separate doubled cw diode Nd:YAG laser ($\lambda = 532\text{ nm}$) for incoherent collisions and is focused onto the sample by means of a spherical $f = 150\text{ mm}$ lens. The setup allows us to vary the mutual (collision) angle α at which the two soliton beams intersect in the crystal. Photographs of the input and output intensity distributions are taken by imaging the input and output facets of the sample onto a CCD camera. We get rid of the output background illumination by means of an x -polarization analyzer before the camera.

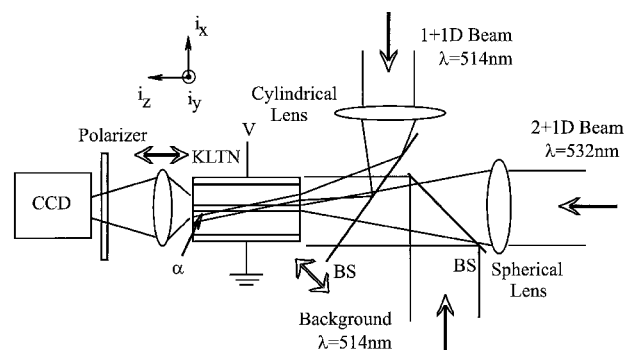


Fig. 1. Experimental setup: BS's, beam splitters; other abbreviations defined in text.

The two-beam operation point is found at $\alpha = 0^\circ$, displacing the two soliton beams far apart to prevent their interaction (i.e., noninteracting parallel propagation). Given a value of V and a background illumination I_b , and having fixed the physical FWHM of the input needle and slab beams (Δx_n and Δx_s , respectively), we vary the peak intensities (independently) of the two beams (I_n and I_s , respectively). Simultaneous soliton formation for $V \cong 1.4$ kV, $\Delta x_n \cong 12$ μm , $\Delta x_s \cong 10$ μm , and amplitude ratios $u_n = (I_n/I_b)^{1/2} \cong 2.2$ and $u_s = (I_s/I_b)^{1/2} \cong 1.6$ is evident from Fig. 2.

In Fig. 3 we show the results of two qualitatively distinct cases that involve incoherent collisions, one for $\alpha \cong 2^\circ$ and the other for $\alpha \cong 1.3^\circ$. In the first case, the needle and slab solitons maintain their self-trapped characteristics after the collision, whereas in the second case, for the smaller angle, the output beams are appreciably distorted (the output evolution does not refer to final asymptotic states because the system is observed less than two diffraction lengths after the collision point). In particular, the slab beam in proximity to the needle (along the y axis) is destabilized, breaking its slab symmetry, whereas the needle is elongated in the y direction, losing its circular symmetry. Discernible distortion was observed for values of $\alpha < 1.5^\circ$. For values of $\alpha > 1.5^\circ$ the self-trapped structure survives the interaction unchanged. For such scattering conditions the pulses behave as quasi-rigid solitons.

A rough estimate of the critical angle can be given in terms self-induced waveguides: Light can pass from one soliton to the other, seeding interaction, when relative scattering angle α is comparable with angular apertures θ_c of the single waveguides.⁶ We can approximately identify θ_c with the equivalent (complementary) critical angle⁷ defined by the relationship $\cos \theta_c \cong (n - \Delta n)/n$, where $\Delta n \cong (1/2)n^3 g_{\text{eff}} \epsilon_0^2 (\epsilon_r - 1)^2 (V/L)^2 \{1 - [1/(1 + u^2)]^2\}$, ϵ_0 is the vacuum dielectric constant, L is the distance between the electrodes ($L = 3.7$ mm), and $u = u_s$ for slab solitons and $u = u_n$ for needle solitons. In our conditions we obtain $\theta_c \cong 1^\circ$ for the slab structure and $\theta_c \cong 1.2^\circ$ for the needle and expect significant coupling for $\alpha \approx \theta_c$, as observed.

Perhaps the crucial physical difference between conventional soliton scattering (see, e.g., Ref. 1) and the system under investigation is the fact that the interaction force, because of the interference in the light caused by overlap of soliton tails, is inherently inhomogeneous; it is strongest in the direction of the shortest soliton separation. The presence of soliton-soliton interaction indicates both rupture of the lower-dimensional symmetry of the slab and distortion of the radial symmetry of the needle. To study the interaction in its most general manifestation, we pass to the investigation of coherent beam coupling. In conventional soliton phenomenology, coherent interactions depend strongly on relative phase; they are attractive for in-phase pulses and repulsive for out-of-phase ones.^{1,2} Coherent slab and needle particles are obtained from the same argon-ion laser in a balanced Mach-Zehnder-like configuration. We measure phase by observing the fringe pattern that results from interference with the background beam simply by rotating the polarizer before the CCD

camera by 45° ; fine adjustments permit tuning of the relative phase. The needle and the slab are launched at $\alpha \cong 0^\circ$ with a peak-to-peak distance of approximately 20 μm , and results are shown in Fig. 4. In Fig. 4(b) the relative phase between the needle and the slab input wave fronts is $\Delta\phi_0 \cong \pi$, and during nonlinear propagation the two particles locally inhomogeneously repel each other, leading to a repulsive-type warping. In Fig. 4(e), $\Delta\phi_0 \cong 0$, and the warping is attractive. Figures 4(c) and 4(d) show the single trapped beam shapes with, respectively, the needle and the slab beams blocked for the repulsive case, whereas Figs. 4(f) and 4(g) refer to the attractive case. Figures 4(c) and 4(d) and Figs. 4(f) and 4(g) refer, respectively, to the same physical situation illustrated in Figs. 4(b) and 4(e), as they are taken

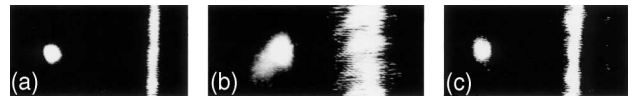


Fig. 2. Hybrid working point: at $T = 21^\circ\text{C}$ and $V = 1.4$ kV the crystal supports independent parallel formation of 130- μm distant needle (left) and slab (right) solitons: (a) input light distribution, (b) diffracted output ($V = 0$) with $\Delta x_{n,s} \cong 24$ μm , (c) output self-trapped light distribution.

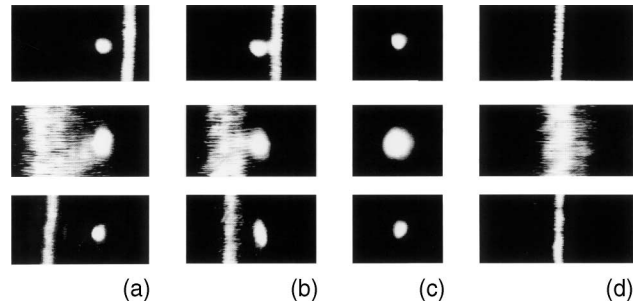


Fig. 3. Hybrid soliton collisions: (a) noninteracting case for $\alpha \cong 2.0^\circ$, (b) interacting case for $\alpha \cong 1.3^\circ$, (c) single-needle soliton, (d) single-slab soliton. Top, middle, and bottom rows: input, diffracted output at $V = 0$, and soliton output at $V = 1.4$ kV, respectively.

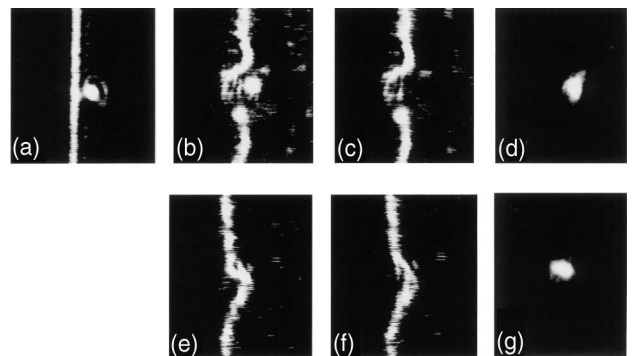


Fig. 4. Coherent interaction: (a) input, (b) output in the repulsive case $\Delta\phi_0 = \pi$, (e) output in the attractive case $\Delta\phi_0 = 0$; (c), (d) same as (b) with needle and stripe, respectively, blocked; (f), (g) same as (e) with needle and stripe, respectively, blocked.

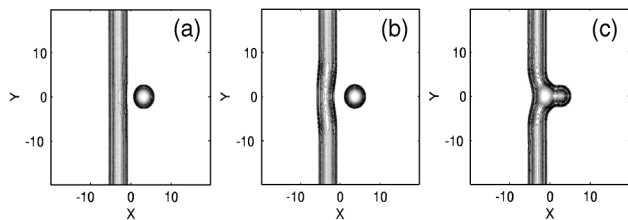


Fig. 5. Slab-needle coherent interaction governed by Eq. (1): (a) input (amplitudes $u_s = 1.3$ and $u_n = 2$), (b) output at $z = 10$ with $\Delta\phi_0 = \pi$, (c) output at $z = 10$ with $\Delta\phi_0 = 0$.

before the system is allowed to evolve to the stationary single-soliton state (typical relaxation times range from a few seconds to minutes, depending on the intensities). Figures 4(c) and 4(d) show how repulsion leads to a substantial distortion of the stripe soliton away from the needle and to a deformation of the needle, suggesting a compression in the transverse x direction. In the attractive case [Figs. 4(f) and 4(g)] the warping is reversed, and the needle is slightly elongated in the x direction.

A detailed and quantitative modeling of the specific nonlinear interaction is beyond the scope of this Letter. Nevertheless, to demonstrate that the basic features of hybrid interaction driven by inhomogeneous forces do not depend on specific features of the nonlinear response of the photorefractive sample, we investigated numerically the dynamics governed by the generalized 2 + 1D local nonlinear Schrödinger equation, which can be put in the dimensionless standard form

$$i \frac{\partial u}{\partial z} + \frac{1}{2} \Delta_{\perp} u + f(|u|^2)u = 0, \quad (1)$$

where $\Delta_{\perp} = \partial_x^2 + \partial_y^2$. We take a local saturable nonlinearity $f(|u|^2) = |u|^2/(1 + \gamma|u|^2)$, which can also be regarded as a local approximate model for screening nonlinearities (significant differences in photorefractive crystals might arise from the anisotropic nature of the nonlinearity; see, e.g., Ref. 14). Needle and stripe solitary solutions of Eq. (1) are found numerically as $u = u_s(x)\exp(i\beta_s z)$ and $u = u_n(x, y)\exp(i\beta_n z)$, respectively. Here, a given value of propagation constant β_n or β_s fixes both peak amplitude and width of the soliton. The interaction is simulated by means of the initial condition $u(x, y, z = 0) = u_s(x - x_0) + u_n(x + x_0, y)\exp(i\Delta\phi_0)$ in Eq. (1). A typical outcome obtained for $\beta_s = \beta_n = 0.4$ (i.e., peak amplitudes $u_s = 1.3$ and $u_n = 2$ with $\gamma = 1$) and a soliton input separation $2x_0 = 6.25$ is illustrated in Fig. 5. As shown, the stripe-needle coherent interactions resemble qualitatively those observed experimentally. Similar results are obtained for $\beta_s \neq \beta_n$, provided that the phase slippage $\Delta\phi(z) - \Delta\phi_0 = (\beta_n - \beta_s)z$ remains negligible over the characteristic distance z where soliton forces are exerted. This constraint is usually fulfilled for well-separated solitons of comparable peak amplitudes, as those employed in the experiment. Otherwise, solitons experience periodic changes from repulsion to attraction.

The observed phenomenology opens up a new family of hereto unexplored configurations whose description involves a series of modeling riddles. Especially intriguing are the search for hybrid bound states and the influence of the collision on single-soliton instabilities. In the latter respect, we point out that the symmetry-breaking short-scale interaction with the needle inhibits any transverse instability of the stripe.¹⁵ In the pure Kerr case, the question of whether the soliton force can arrest collapse of the needle remains open. Finally, the index pattern induced in the crystal can be used at nonphotorefractively active wavelengths (i.e., $\lambda > 0.6 \mu\text{m}$) to investigate directional coupling based on the hybrid resonance¹⁶ and produce a tunable fiber-waveguide coupler as a remarkable extension of soliton-based slab-slab couplers.¹⁷

We thank M. Segev and Y. Kivshar for useful discussions and suggestions. The research of E. DelRe was carried out in the framework of an agreement between the Fondazione Ugo Bordoni and the Italian Communications Administration; that of A. J. Agranat was supported by a grant from the Ministry of Science of the State of Israel. E. DelRe's e-mail address is edelre@fub.it.

References

1. J. P. Gordon, *Opt. Lett.* **8**, 596 (1982).
2. F. Reynaud and A. Barthelemy, *Europhys. Lett.* **12**, 401 (1990).
3. J. S. Aitchison, A. M. Weiner, Y. Silberberg, D. E. Leaird, M. K. Oliver, J. L. Jackel, and P. W. E. Smith, *Opt. Lett.* **16**, 15 (1991).
4. S. Wabnitz, Y. Kodama, and A. B. Aceves, *Opt. Fiber Technol.* **1**, 187 (1995).
5. K. A. Gorshkov and L. A. Ostrovsky, *Physica D* **3**, 428 (1981).
6. A. W. Snyder and A. P. Sheppard, *Opt. Lett.* **18**, 482 (1993).
7. M. Shih, Z. Chen, M. Segev, T. H. Coskun, and D. N. Christodoulides, *Appl. Phys. Lett.* **69**, 4151 (1996).
8. H. Meng, G. Salamo, M. Shih, and M. Segev, *Opt. Lett.* **22**, 448 (1997).
9. G. S. Garcia-Quirino, M. D. Iturbe-Castillo, V. A. Vysloukh, J. J. Sánchez-Mondragón, S. I. Stepanov, G. Lugo-Martinez, and G. E. Torres-Cisneros, *Opt. Lett.* **22**, 154 (1997).
10. A. V. Mamaev, M. Saffman, and A. A. Zozulya, *J. Opt. Soc. Am. B* **15**, 2079 (1998).
11. M. Segev, M. Shih, and G. C. Valley, *J. Opt. Soc. Am. B* **13**, 706 (1996).
12. E. DelRe, B. Crosignani, M. Tamburrini, M. Segev, M. Mitchell, E. Rafaeli, and A. J. Agranat, *Opt. Lett.* **23**, 421 (1998).
13. E. DelRe, M. Tamburrini, M. Segev, E. Rafaeli, and A. J. Agranat, *Appl. Phys. Lett.* **73**, 16 (1998).
14. W. Krolikowski, M. Saffman, B. Luther-Davies, and C. Denz, *Phys. Rev. Lett.* **80**, 3240 (1998).
15. E. A. Kuznetsov, A. M. Rubenchik, and V. E. Zakharov, *Phys. Rep.* **142**, 103 (1986).
16. D. Marcuse, *J. Lightwave Technol.* **7**, 122 (1989).
17. S. Lan, E. DelRe, Z. Chen, M. Shih, and M. Segev, *Opt. Lett.* **24**, 475 (1999).